Enhancement and Segmentation of Vascular Structures for Biological Image Analysis

A Dissertation

Presented to

The faculty of the School of Engineering and Applied Science

University of Virginia

In partial fulfillment

of the requirements for the degree

Doctor of Philosophy (Electrical and Computer Engineering)

by

Suvadip Mukherjee

July 2015

Approval Sheet

This dissertation is submitted in partial fulfillment of the requirements for the degree of Doctor of Philosophy (Electrical and Computer Engineering)

Author: Suvadip Mukherjee

This dissertation has been read and approved by the examining committee:

Scott T. Acton, Dissertation Adviser

Stephen G. Wilson, Committee Chair

Zongli Lin, Committee Member

Connelly Barnes, Committee Member

Barry G. Condron, Committee Member

Accepted for the School of Engineering and Applied Science:

Dean, School of Engineering and Applied Science

July 2015

Abstract

This is the abstract page which I will write shortly

Contents

List of Figures

List of Tables

Symbols

a	Scalar notation
$\mathbf{a}$	Vector notation
[A]	Matrix notation
Ω	Domain of the image function ($\Omega \subset \mathbb{R}^2/\mathbb{R}^3$)
$\mathbf{x}$	Position vector (x,y) or (x,y,z) $\in \Omega$
$*$	Convolution operator
$\cdot$	Vector dot product operator
t	Scalar variable denoting time/pseudo time
σ	Scale parameter
$f(\mathbf{x})$	Continuous image function, $f : \Omega \mapsto \mathbb{R}$
$g_\sigma(\mathbf{x})$	Zero mean isotropic Gaussian kernel, with std. deviation σ
∇	Gradient operator
$\text{div}(\mathbf{a})$	Divergence operator, $\nabla \cdot \mathbf{a}$
∇^2	Laplacian operator
$N_\sigma(\mathbf{x})$	*Vesselness* response at scale σ
$N(\mathbf{x})$	Scale-space *vesselness* response
$\mathcal{H}_\sigma(\mathbf{x})$	Hessian matrix of $f(\mathbf{x}) * g_\sigma(\mathbf{x})$
$\phi(\mathbf{x}, t)$	Level set function, $\phi : \Omega \times \mathbb{R}^+ \mapsto \mathbb{R}$
$H(\phi)$	Heaviside function
$\delta(\phi)$	Dirac delta function
$\mathbf{C}(p)$	Parametric curve, $p \in \{0, 1\}$
$\mathbf{C}_t$	$\dfrac{\partial \mathbf{C}}{\partial t}$
$\mathbf{n}$	Unit outward normal vector to a curve
$\mathbf{t}$	Unit tangent vector to a curve
$\mathcal{P}_k(\mathbf{x})$	Legendre polynomial of degree k
$\mathbb{P}(\mathbf{x}) = (\mathcal{P}_0(\mathbf{x}), \ldots, \mathcal{P}_N(\mathbf{x}))^T$	Vector of Legendre polynomials

Chapter 1

Introduction

Recent years have witnessed an increasing trend in collaborative research between the field of biological sciences and engineering. In particular, advances in modern day imaging techniques have enabled biologists to image cellular and subcellular structures over a vast range of spatial resolution, ranging from micrometer to nanometer scale. Using state of the art imaging protocols, biologists are now able to generate image data at an unprecedented scale. However, while imaging is no longer considered a bottleneck for experimental biology, the sheer volume of data being collected calls for automated processing for high throughput study in cell biology. This has established a new field of interdisciplinary research – *Bioimage Informatics* [4], leading to a number of cross disciplinary publications as well as software suits for image processing techniques which are specialized for such biological tasks [5–7].

1.1 Neuroimage analysis

A subcategory of the aforementioned discipline of bioimage informatics involves image analysis for neuroscience. Researchers in this field of *Neuroimage analysis* borrow techniques from digital image analysis and computer vision for deeper understanding of the brain's functionality (for a model organism) through image based studies.

Functions of an animal's brain are largely governed by its neurons, and the number of neurons vary between a few hundreds in the roundworm *C. elegans* [8] to a hundred billion in an adult human brain. The relationship between the morphology and functionality of neurons was established by Ramon Y Cajal in the 19th century. Cajal's hypothesis serves as the basis for modern day neuroimage analysis. Studies based on morphological properties of individual neurons and neuronal components such as dendritic spines, synapses, mitochondria etc. have shown promise in better understanding and diagnosis of various neurological disorders and neuro-degenerative diseases [9–13]. It is evident that neuroimage analysis becomes a big data problem as we prepare ourselves to study the nervous system of vertebrates. This suggests that the prevalent norm of data interpretation by a trained human personnel needs to be replaced with sophisticated automation. It is not surprising that this problem has been receiving significant attention over the last few years. For example, the publicly accessible website *neuromorpho.org* [14] was published in 2006 with only a few hundreds of neurons in its repository. As of June 2015, neuromorpho.org contains more than ten thousand digitally reconstructed neurons, contributed by researchers from over 120 laboratories worldwide.

Two basic steps are involved in designing a platform for image based study of the brain – image acquisition and image analysis [15].

1.1.1   Image Acquisition

Choice of a particular imaging modality depends on the specific application. Fluorescence microscopy is a popular choice when the study involves a global structural analysis of the neurons or some neuronal components in the micrometer scale. For such imaging techniques, the specimen is genetically tagged with a fluorescence protein (GFP, YFP etc.) which emits photons when illuminated by a light source [12]. These photons are eventually detected by a sensor to produce a digital image of an optical plane. Laser

scanning confocal microscopes are commonly used for fast three dimensional imaging of neurons of model animals such as Drosophila, rat, mice etc. Depending on the application, other imaging techniques such as bright-field microscopy [16], multiphoton microscopy [17] etc. are also used to image neuronal structures. Electron microscopy (EM) is a popular choice for imaging neuronal structures at nanometer scale. EM is particularly useful in analyzing subcellular objects and surrounding structures such as mitochondria, synapse, vesicles etc. Focus Ion Beam Scanning Electron Microscopy (FIBSEM) [18] can now deliver near isotropic 3D images with extremely high resolution and is slowly being the imaging modality of choice for nano-scale analysis of neuronal structures.

1.1.2 Image analysis

While we are still far away from achieving our end goal of understanding the brain, recent research suggest that detection and quantification of morphological anomalies of some neuronal structures can answer some relevant questions related to diagnosis of certain neural disorders. Specifically, morphological structure of individual neurons, dendritic spines and certain characteristics of subcellular objects such as synapses, mitochondria etc. reveal important information regarding the brain's functioning. Anomaly quantification can be performed via comparison of the shape of the structures, which in turn requires a robust segmentation technique. Broadly, the relevant research in neuro-image analysis can be categorized into the following groups: segmentation and shape analysis of individual neurons [1, 2, 19–21], study of the types of dendritic cells and characteristics of the intra neuronal structures [22–25]. While the end goal remains the same, all these methods differ considerably from the engineering point of view and require different imaging modalities. As a result, the processing algorithms differ considerably in nature, thus making each of these techniques individual topic of extensive research.

1.2   Problem formulation

In the recent years there have been concerted efforts to develop analytic models for global morphological comparisons of neurons. This is because anatomical distortion of neurons provide initial clues toward neurological disease understanding, diagnosis or monitoring. This refers to the branch of study where the geometric and morphological properties of single neuron cells are studied for better understanding of its functioning. Since it is widely believed that structural anomaly of neurons correlate well with changes in its functioning, such global morphological assessments are essential for performing tasks such as quantification of the neuron degeneration due to a disease or drug usage, identifying young and adult neurons in the brain, differentiating between cells in different layers of the brain etc. [9–13, 26].

Designing a workflow for the aforementioned global shape based study involves two critical steps. First, a digital reconstruction should be obtained from the raw image data. This is the segmentation or tracing stage. Automated algorithms for performing high throughput digital reconstruction is crucial in developing building the neuronal atlas for a species. Till date, such an atlas exists for the round worm *C. elegans* [8], where the neurons exhibit significantly simpler structural patterns. However, for developed species such as the fruit fly, mice, zebrafish, huumans, *etc.* developing such shape based neuron atlas is still an unsolved problem.

Having a shape based neuronal atlas for an animal would open doors for further statistical studies based on the neuronal anatomy. Also, digital reconstructions allow us to mathematically compare the cell shapes for detecting morphological anomalies. It turns out that both these sub-problems come with their own sets of challenges and complications and deserve to be treated separately.

The pertinent challenge for global structural analysis is to develop appropriate pipeline

for identification and quantification of the morphology of a single neuron. Confocal microscopy is generally the chosen modality for imaging, since the entire neuron cell can be imaged in the micrometer resolution. Neuron reconstruction (or tracing) refers to the problem of acquiring the neural anatomy from microscopy. Image processing is challenging both due to the structural complexity of neurons as well as due to imaging artifacts such as poor contrast, presence of non-neuronal clutter and low signal to noise ratio of the images.

This dissertation addresses the problem of developing automated algorithms for segmenting single neurons from 2D and 3D microscopy data. The final goal is to construct digital reconstruction of the neurons, so that their structural pattern can be embedded in a mathematical structure for future shape based comparisons. Furthermore, automated algorithms are necessary for developing the "Neurome" or atlas of neurons for a model organism for future studies.

We demonstrate the applicability of our developed methods primarily on neuron images of the fruit fly *Drosophila*, which are imaged in Dr. Barry Condron's laboratory at the University of Virginia (Department of Biology). Since developing imaging protocols is not one of our aims, we briefly discuss the image acquisition step in the following segment.

1.2.1   Single neuron imaging

We are interested in investigating the morphological properties of single neurons of the fruit fly Drosophila. A detailed survey of the imaging protocols is elaborate, and is out of scope of this dissertation. However, a brief summary of the imaging method is discussed here to understand on the dataset that we will be using for analyzing our algorithms.

Biologists have shown interest in studying the neuronal processes (axons, dendrites, synapses etc.) of the Drosophila, which has been a preferred model organism for to study genetics and developmental biology for several years. The central nervous system (CNS)

(a)   (b)   (c)
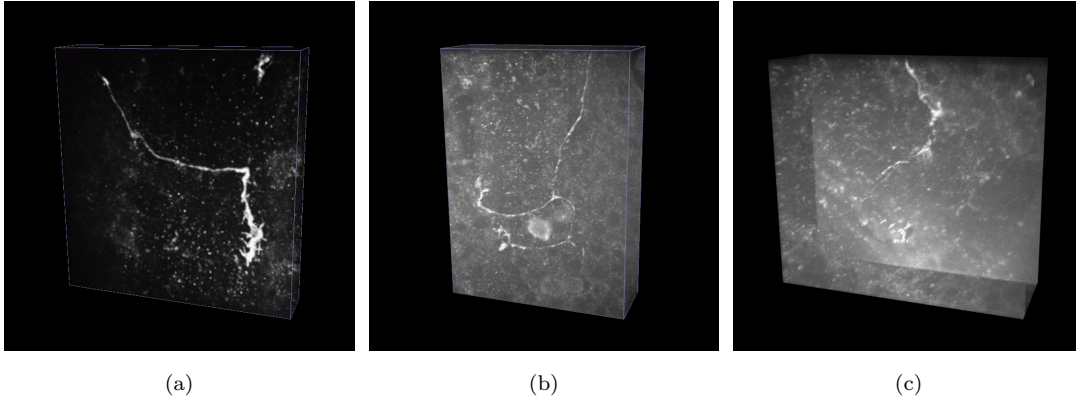
FIGURE 1.1: Drosophila neurons imaged by confocal microscope. (a) is a low SNR sensory neuron. The background clutter are due to illuminated non neuronal filaments. (b) and (c) are interneurons, the image quality severely degraded by photon noise, low signal intensity and in-homogeneous contrast.

of the Drosophila contains a vast array of interacting synapses and neuronal processes in addition to containing about 20,000 neurons in the larval stage.

Green Florescence Protein (GFP) is used to label the neuronal cells, which are produced through a combination of a FLP/FRT system and GAL4/UAS system. Approximately 10 hr old embryos were heat shocked at 37°C for 1-2 hrs, that generates single GFP-labeled cells [11]. Using this protocol, most Ventral Nerve Cord (VNC)'s have about 5 labeled cells, thus allowing for imaging of individual neurons.

For imaging the labeled cells, confocal microscopy was used to image the cells in three dimensions, with resolution in the micrometer range. Three images captured in the Condron Lab at the University of Virginia are shown in Fig. 1.1

1.3   Contributions of this thesis

The major emphasis of this dissertation will be on developing novel algorithms for segmenting single neurons from confocal microscopy data. We realize that a large scale structural analysis of neuron groups demand efficient, automated segmentation to generate the digital morphology. Therefore, in this work, we primarily focus on developing

and improving the first stepping stone for *neuromics*– automated neuron segmentation algorithms.

Contribution 1: Graph theoretic neuron segmentation

We devise a novel neuron tracing technique Tree2Tree-2 [20], which combines the strengths of variational segmentation and graph based connectivity analysis of disjoint connected components. We also introduce a novel methodology to generate a *medialness* function [27] for tubular objects, for the purpose of obtaining a smooth tracing along the neuron centerline.

Contribution 2: Region based 2D segmentation with level sets

2D analysis often serves as a preliminary step for understanding the anatomy of neurites. Furthermore, certain categories of neurons (e.g. sensory neurons on the cuticle layer of *Drosophila* larva) are topologically flat and therefore, the third dimension of imaging does not yield useful information for analysis. In this regard, we have developed a general purpose segmentation algorithm which uses geometric active contours. The proposed algorithm, *Legendre Level Set* (L2S) [28] aims at segmenting the objects from microscopy images in presence of heterogeneous illumination.

Contribution 3: Tubularity field based 3D segmentation with level sets

We propose a novel neuron tracing architecture, Tubularity Flow Field (TuFF) [21], which uses geometric active contours to perform segmentation guided by the local tubularity of the neurites. One advantage of using geometric active contours is that these techniques are adaptive to the topology of the objects. As a result, joining disjoint neurites can be handled in a natural framework unlike Tree2Tree-2, where error is often introduced in the solution due to improper connectivity handling. We also provide a mechanism to combat

the sporadic signal loss across the structures by incorporating a specialized attraction force in our solution to merge nearby fragments.

1.4   Thesis outline

The rest of the dissertation is organized as follows: In Chapter 2, we discuss popular neuron segmentation techniques, as well as relevant methodologies for pre-processing. The graph based segmentation algorithm is discussed in Chapter 3 and the results are scrutinized for both 2D and 3D data. We identify the pros and cons of our method and discuss the motivation of using geometric active contours for more flexibility in establishing component connectivity.

In Chapter 4, a brief summary of geometric active contours is presented, followed by discussion of the proposed 2D segmentation method L2S in Chapter 5. The 3D segmentation case using TuFF is presented in Chapter 6, along with strategies to improve segmentation results using a robust non local vessel detection technique. Finally, we conclude in Chapter 7 with discussion of the methods, their future extensions and possible applications.

Apart from the aforementioned primary contributions, we found that the developed algorithms are quite general, and have a wide variety of applications involving vascular structures. Two such applications are discussed in the Appendix; the first one involves segmenting human arteries from low SNR ultrasound imagery, and the second method relates to the civil engineering discipline, where the goal is to detect cracks in concrete structures such as bridges and pavements.

1.5   Publications resulting from this work

Journal Publications

- **S. Mukherjee**, B. Condron and S.T. Acton, "Tubularity Flow Field – A Technique For Automatic Neuron Segmentation," *IEEE Transactions on Image Processing*, vol.24, no.1, pp.374,389, Jan. 2015

- **S. Mukherjee** and S.T. Acton, "Region Based Segmentation in Presence of Intensity Inhomogeneity Using Legendre Polynomials," *IEEE Signal Processing Letters*, vol.22, no.3, pp.298,302, March 2015

- R.Sarkar, **S. Mukherjee** and S.T. Acton, "Dictionary Learning Level Sets" *IEEE Signal Processing Letters* (*under minor revision*)

- **S. Mukherjee**, L. Boulton and S.T. Acton, "Concrete crack detection using edge assisted Tubularity Flow Field with local directional evidence", *in preparation.*

CONFERENCE PUBLICATIONS

- **S. Mukherjee** and S.T. Acton, "Oriented Filters for Vessel Contrast Enhancement With Local Directional Evidence", *IEEE ISBI 2015* (accepted).

- M. Consylman, **S. Mukherjee**, D.P. Mukherjee, B. Condron and Scott T. Acton, "Social behavior analysis of Drosophila larvae via motion activity recognition", *IEEE SSIAI 2014.*

- **S. Mukherjee**, B. Condron and S.T. Acton, "Neuron segmentation with level sets", *ACSSC 2013*:1078-1082

- R. Sarkar, **S. Mukherjee** and S. T. Acton, "Shape descriptors based on compressed sensing with application to neuron matching", *ACSSC 2013*: 970-974

- **S. Mukherjee** and S. T. Acton, "Vector field convolution medialness applied to neuron tracing," *ICIP 2013*: 665-669

- **S. Mukherjee**, B. Condron and S. T. Acton, "Chasing the neurome: Segmentation and comparison of neurons," *EUSIPCO 2013*: 1-4

- **S. Mukherjee**, S. Basu, B. Condron and S.T. Acton , "Tree2Tree2: Neuron tracing in 3D," *ISBI 2013*: 448-451

- **S. Mukherjee**, S. Basu, B. Condron and S.T. Acton, "A geometric-statistical approach toward neuron matching", *ISBI 2012*: 772-775.

Appendix A

Dictionary Learning Level Set

A.1 Dictionary Learning Level Sets (DL2S)

The primary motivation for DL2S is similar to that of L2S– performing segmentation in presence of intensity inhomogeneity. In L2S [28], we generalized the Chan-Vese model by approximating the foreground and background regions as a piecewise polynomial function computed via linear combination of a few Legendre basis functions. This can be viewed from the perspective of low dimensional approximation of a signal. While Chan-Vese's method is a form of extreme dimensionality reduction (due to the piecewise constant assumption), L2S achieves a balance between reduction of dimensionality and accurate intensity modeling.

Despite its merits, L2S suffers from certain issues. First, the segmentation quality relies heavily on the number of chosen basis functions. Second, L2S suffers from scalability issues since the pre-specified bases cannot represent any arbitrary intensity variation. As it turns out, recent research in the field of sparse modeling and dictionary learning [108, 113–116] have shown that for a given set of training data, one can obtain an optimal set of basis elements (atoms) to represent a signal. This is the main highlight of DL2S *–instead of explicitly specifying the set of basis elements, we estimate an optimal set of*
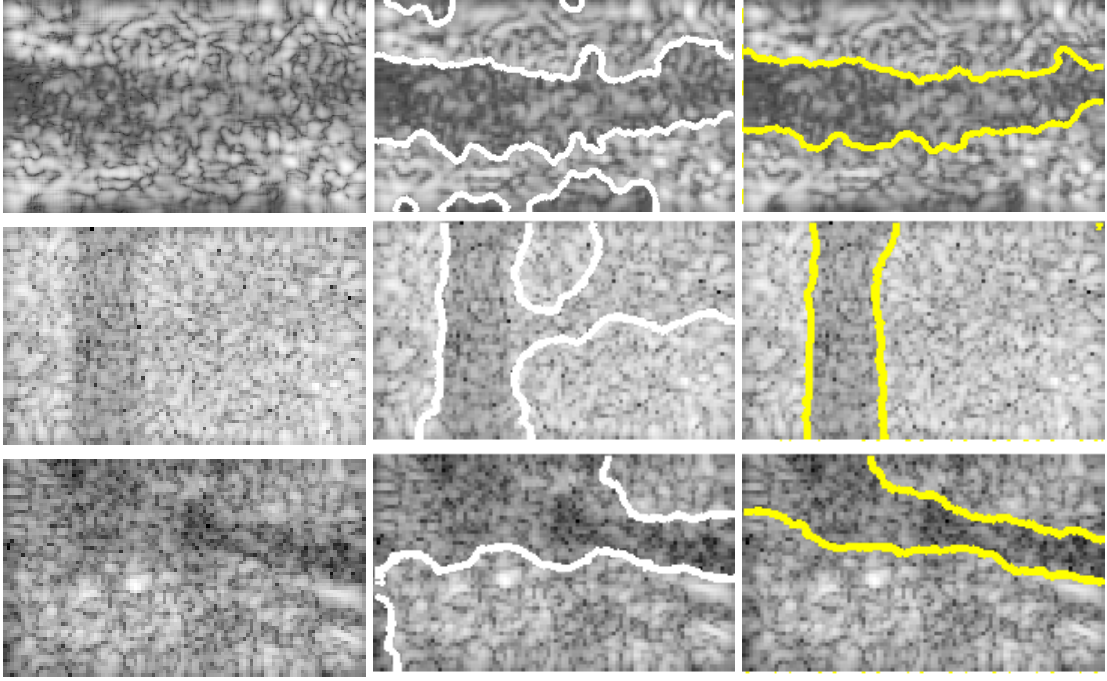
FIGURE A.1: Segmentation results of Chan-Vese [88] (white) and DL2S (yellow) on three C-mode ultrasound images captured with a portable scanner.

bases from the set of training images using dictionary learning. To demonstrate our technique, we choose an important segmentation problem for ultrasound imaging. Blood vessels are imaged in C-mode using a portable, low cost, battery operated ultrasound device. Our objective is to segment the vessel boundary to assist medical practitioners for performing phlebotomy application such as intravenous needle placement (see Fig. A.1). Images captured using these portable devices suffer from low contrast, noise and speckle in addition to non-linear illumination of the objects which makes segmentation challenging.

A.1.1 Methodology

A generalized version of Chan-Vese's model can be formulated as follows:

$$
\begin{aligned}
\mathcal{E}(\phi, A, B) \;\; &= \int_\Omega |f(\mathbf{x}) - \sum_{i=0}^k a_i d_i(\mathbf{x})|^2 m_1(\mathbf{x}) d\mathbf{x} + \int_\Omega |f(\mathbf{x}) - \sum_{i=0}^k b_i d_i(\mathbf{x})|^2 m_2(\mathbf{x}) d\mathbf{x} \\
&\quad + \nu \int_\Omega |\nabla H_\epsilon(\phi)| d\mathbf{x} + \lambda \left(||A||_2^2 + ||B||_2^2 \right)
\end{aligned}
\tag{A.1}
$$

Here $\mathbb{D}_k(\mathbf{x}) = [d_1(\mathbf{x}), \ldots, d_k(\mathbf{x})]^T$ is a dictionary which will be discussed in detail shortly. $d_0(\mathbf{x}) = \mathbf{1}$. $d_1, \ldots, d_k$ are dictionary elements or atoms which are used to model the non-linearity in the intra-region intensities of the images. The third term in (A.1) introduces smoothness in the solution, which is controlled using the parameter ν. $\mathbf{a} = [a_0, \ldots, a_k]^T$, $\mathbf{b} = [b_0, \ldots, b_k]^T$ are $(k+1)$ dimension real valued coefficient vectors. The parameter λ reduces over-fitting, by constraining the ℓ_2 norm of the coefficient vectors.

With $k = 0$, (A.1) reduces to the piecewise constant model in (4.18). In other words, (A.1) generalizes the traditional Chan-Vese technique by introducing capability to handle heterogeneous image regions. Here $d_1, \ldots, d_k$ can be interpreted as *detail functions* to model the intensity variation in conjunction to the constant illumination term d_0. As earlier, (A.1) can be optimized with respect to ϕ, A and B using alternating minimization.

Naturally, a question arises– how to select $d_1(\mathbf{x}), \ldots, d_k(\mathbf{x})$? It was shown in [28] that high quality segmentation results can be obtained by using a few Legendre basis functions. However, we hypothesize that if a dataset of example images is available, we can enhance the segmentation performance by learning an optimal set of basis functions (dictionary elements) for region intensity approximation instead of using a predefined set of basis. For the application described in this paper, we are concerned with sets of ultrasound images, imaged using similar type of devices. The multi-depth images are captured at the same scale, and are preregistered. As a result, we have the provision to learn these functions $d_i(\mathbf{x})$ directly from the dataset, rather than relying on *ad hoc* procedures for selecting the same.

A.1.2 Intensity modeling with dictionary learning

Sparse coding techniques have gained popularity recently. Such algorithms have been used for a multitude of applications ranging from image denoising, inpainting, restoration, classification, retrieval etc [113–116]. Given a set of training data, the goal of dictionary

learning is to compute a set of basis elements, also called *atoms*, such that each training data can be represented as a linear combination of only a few of these atoms. The key idea is to utilize the underlying sparsity of the training data, while minimizing the reconstruction error. Mathematically, if $\mathbb{F} = [\mathbf{f}_1, \ldots, \mathbf{f}_N]$ denotes the set of N discretized, vectorized and mean subtracted training images, we can use dictionary learning technique to compute the dictionary $\mathbb{D}_k = [\mathbf{d}_1, \ldots, \mathbf{d}_k]^T$ mentioned in (A.1) by solving the following optimization problem

$$\mathbb{D}_k = \arg \min_{\mathbb{D}, \mathbf{y}_i} \sum_{i=1}^{N} ||\mathbf{f}_i - \mathbb{D}^T \mathbf{y}_i||_2^2$$
$$\text{such that } ||\mathbf{y}_i||_0 \leq \theta, \quad \forall i = 1, ..., N. \tag{A.2}$$

where y_i is a coefficient vector corresponding to the ith training image and θ is a scalar which dictates the level of sparsity. There are a number of methods in the literature that use some approximation to solve the hard optimization problem (A.2). For example, k-SVD [108] combines a greedy methodology using orthogonal matching pursuit algorithm to provide a fast solution to this problem. Dictionary learning exploits sparsity in the data (A.2) by constraining ℓ_0 norm of the coefficients.

A.1.3   DL2S curve evolution

Let us denote $\hat{\mathbb{D}}_k = [d_0(\mathbf{x})^T \; \mathbb{D}_k(\mathbf{x})]^T$. We first try to minimize (A.1) with respect to A and B, by taking derivatives and setting the result to zero. A closed form solution is obtained as follows:

$$\hat{\mathbf{a}} = \; [K + \lambda \mathbb{I}]^{-1} \int_{\Omega} \hat{\mathbb{D}}(\mathbf{x}) f(\mathbf{x}) m_1(\mathbf{x}) d\mathbf{x} \tag{A.3}$$

$$\hat{\mathbf{b}} = \; [L + \lambda \mathbb{I}]^{-1} \int_{\Omega} \hat{\mathbb{D}}(\mathbf{x}) f(\mathbf{x}) m_2(\mathbf{x}) d\mathbf{x} \tag{A.4}$$
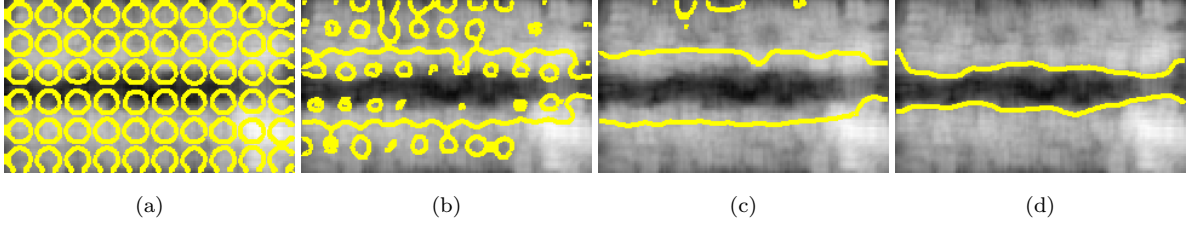
FIGURE A.2: Evolution steps shown for our algorithm (a) initialization, (b) iteration=20, (c) iteration=60, (d) final contour.

where [.] denotes a matrix. $[K]$ and $[L]$ are $k \times k$ Gramian matrices [103], in which $(i,j)^{th}$ entries are obtained as

$$[K]_{i,j} = m_1(\mathbf{x}) \langle d_i, d_j \rangle \text{ and } [L]_{i,j} = m_2(\mathbf{x}) \langle d_i, d_j \rangle \tag{A.5}$$

$0 \leq i, j \leq k$ and $\langle , \rangle$ denotes the Euclidean inner product operator. With the updated coefficient vectors, we can now minimize (A.1) with respect to ϕ using variational calculus. We obtain the following partial differential equation using gradient descent technique for minimization.

$$\frac{\partial \phi}{\partial t} = \left[-|f(\mathbf{x}) - \hat{\mathbf{a}}^T \hat{\mathbb{D}}_k(\mathbf{x})|^2 + |f(\mathbf{x}) - \hat{\mathbf{b}}^T \hat{\mathbb{D}}_k(\mathbf{x})|^2 \right] \delta_\epsilon(\phi) + \nu \delta_\epsilon(\phi) \nabla \cdot \left(\frac{\nabla \phi}{|\nabla \phi|} \right) \tag{A.6}$$

We initialize $\phi|_{t=0} = \phi_0$ and $\dfrac{\delta_\epsilon(\phi)}{|\nabla \phi|} \dfrac{\partial \phi}{\partial \hat{n}} = 0$ at the domain boundary. The gradient flow of DL2S is computed iteratively by discretizing (A.6) using a finite difference scheme. Fig. A.2 shows different steps of the curve evolution. Fig. A.2(a) shows the initialization Fig. A.2(b) and (c) shows two intermediate steps and Fig. A.2(d) shows the finally evolved curve.

A.1.4   Analysis of DL2S

The Chan-Vese method performs segmentation by approximating an image $f(\mathbf{x})$ by a piecewise constant image $g(\mathbf{x})$. To make the model more flexible, we add higher order
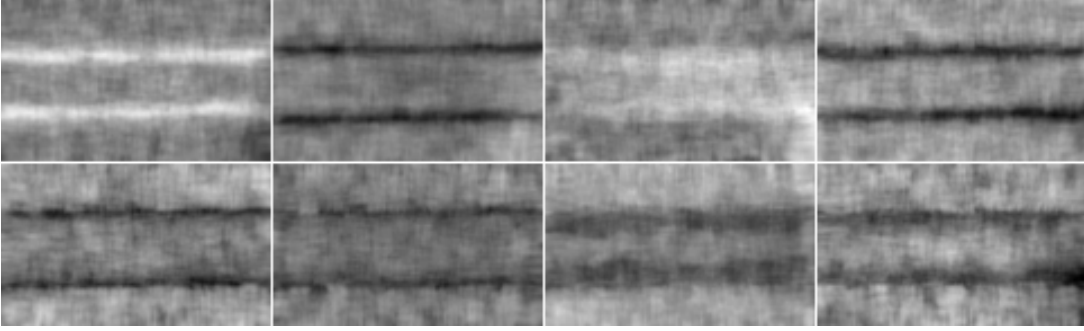
FIGURE A.3: Eight dictionary atoms learned from the mean subtracted images for a phantom image category.

terms which can capture the intensity variations in the regions. Going by the intuition of Chan and Vese, it is fair to approximate the mean image of a dataset as a piecewise constant image.

Assuming a mean image which is approximately piecewise constant, the dictionary atoms learned from the mean subtracted dataset can be utilized to provide the non-linear variation necessary to model the intensity inhomogeneity. The energy functional in (A.1) essentially incorporates this idea in a mathematical framework. One can also think of the dictionary atoms as incorporating higher order details, learned to suit our dataset. The dictionary atoms computed for a particular ultrasound image dataset is shown in Fig. A.3. The dictionary atoms aid in retaining the more significant image properties and compactly represent the dataset.

DL2S is applicable where a set of pre-registered training data is available, for example multi-depth ultrasound images of blood vessels, in temporal image sequences of biomedical objects such as carotid artery, heart videos. In applications involving a temporal image sequence, the first few frames of the can be treated as the training data to learn the dictionary, which can be exploited to segment the subsequent frames.

A.1.5 Experimental Results

We use five different sets of images to evaluate the performance of our algorithm. Out of them, three datasets contain images of medical phantoms which mimic human veins. These phantoms are generally used by medical practitioners for device calibration. The remaining two datasets consists of human vein images, captured *in vivo*. Each dataset contains approximately 18 to 60 images, captured in C-mode using a portable, battery operated ultrasound scanner. The different images in a given set correspond to the image of a vein at various depths. Note that each dataset consists of registered blood vessel images. The vessel orientation and scale are also consistent. A separate dictionary is computed using the mean subtracted images for each of the datasets.

Dependency on contour initialization: We show the performance of our algorithm using both manual and automatic initialization methods. The segmentation results with manual and automatic initialization for Chan-Vese [88], L2S [28] and DL2S are shown in Fig. A.4 for the same image. We observe that the segmentation performance of L2S drops significantly for automatic initialization, which is also true for Chan-Vese method. In comparison DL2S has similar segmentation results for both initialization technique. Quantitative evaluation of performance based on initialization is provided in Table I.

(a)   (b)   (c)   (d)
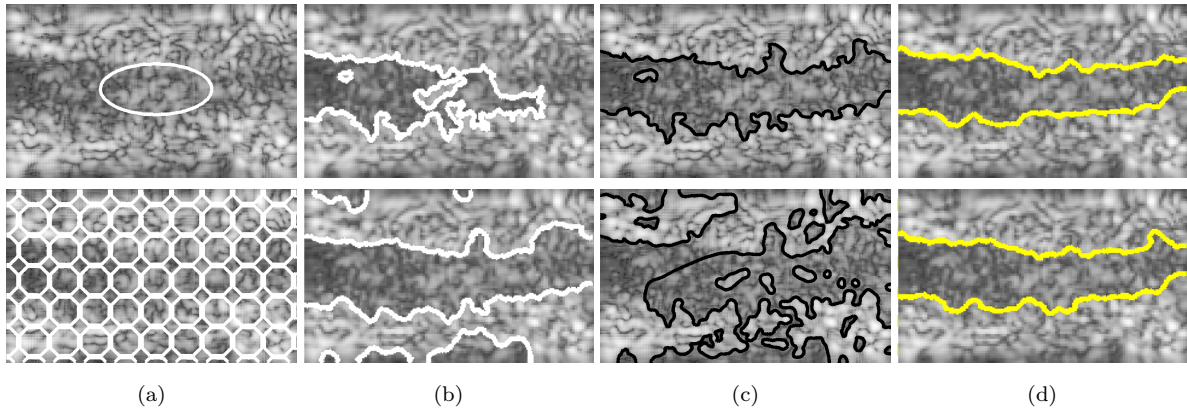
FIGURE A.4: Comparison of segmentation results using manual and automatic initialization methods. (a) initialized contour (b) segmentation results of Chan-Vese (white), (c) segmentation via L2S (black) and (d) segmentation via DL2S model (yellow)
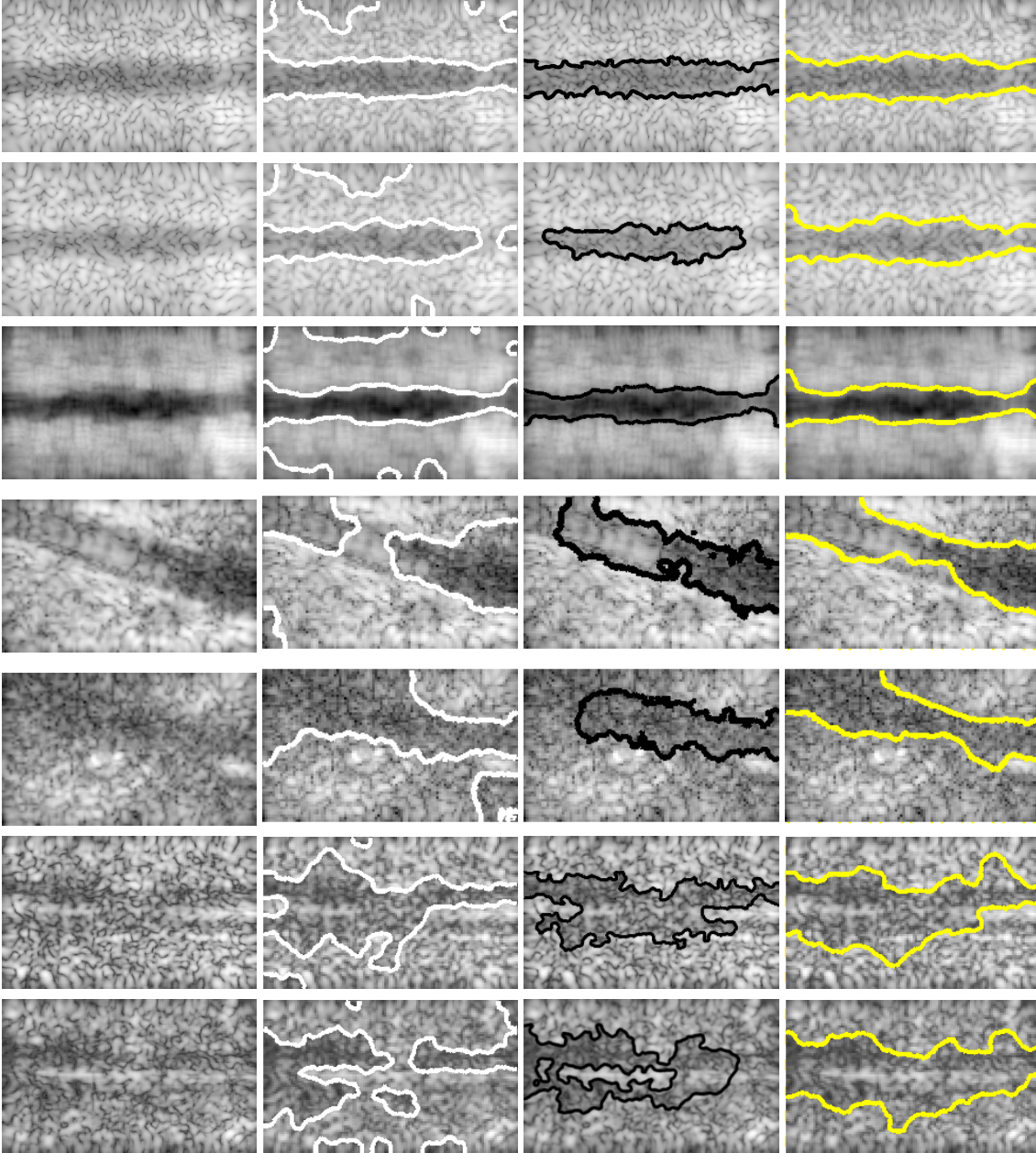
FIGURE A.5: Segmentation comparison of DL2S with Chan-Vese and L2S is shown here. The original C-mode ultrasound images captured with a portable scanner are shown in the first column. Segmentation results of Chan-Vese (white), L2S (black) and DL2S model (yellow) on these images are shown in columns 2, 3 and 4 respectively.

Dependency on dictionary size: We perform sensitivity analysis experiment to study the performance of the segmentation algorithm with changing dictionary size. The Dice coefficient are plotted (along Y-axis) for L2S [28] (Fig. A.6 (a)) ans DL2S (Fig. A.6 (b)) to show the performance with changing basis / dictionary size (along X-axis) for 7 randomly chosen images. In comparison to L2S, where performance decreases with
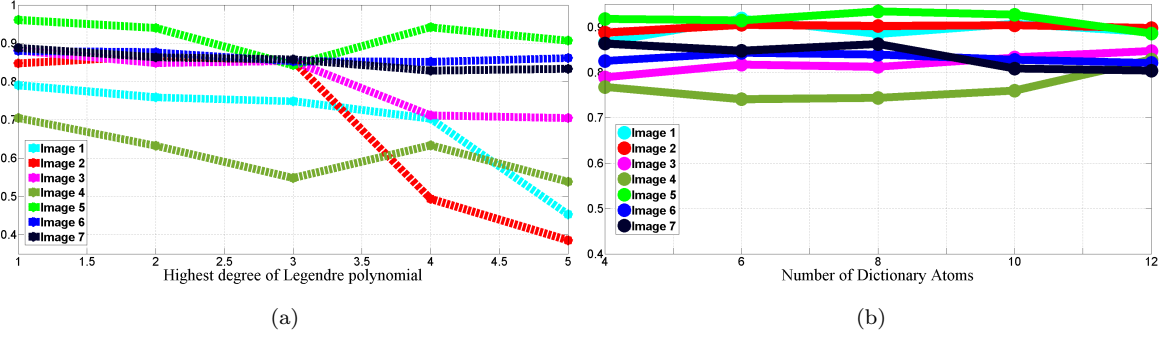
FIGURE A.6: (a) Dice coefficient for L2S with changing number of basis functions, (b) Dice index for the same images plotted for DL2S with changing size of dictionary

increasing number of basis functions, DL2S exhibits a more stable performance. Based on experiment evaluation, we fix the number of dictionary elements $k = 8$ which is at most 50% of the size of the smallest dataset. We choose sparsity inducing parameter $\theta = 3$ such that about 30% or less number of atoms can be used for representing the training images.

Quantitative comparison of segmentation: Fig. A.5 shows the segmentation performance of Chan-Vese (white) [88]), L2S (black) [28] and DL2S (yellow) Fig. A.5 shows that DL2S is able to capture the blood vessels more appropriately in presence of severe contrast and intensity inhomogeneity. A quantitative comparison for five datasets as shown in Table A.1. The Dice index is evaluated for the three algorithms. Here s_g denotes the ground truth segmentation and s_t is the segmentation result for DL2S, Chan-Vese or L2S. It is observed that for each dataset, DL2S demonstrates significantly

TABLE A.1:
Quantitative comparison of the three methods

DL2S		*Chan-Vese* [88]		*L2S* [28]	
Manual	*Auto*	*Manual*	*Auto*	*Manual*	*Auto*
0.93±0.02	0.92±0.04	0.91± 0.07	0.86±0.11	0.89±0.09	0.55±0.17
0.90±0.04	**0.90±0.07**	0.88± 0.05	0.88±0.12	**0.90±0.06**	0.88±0.12
0.85±0.08	**0.86±0.08**	0.80± 0.08	0.85±0.11	0.85±0.12	0.84±0.09
0.80±0.10	**0.83±0.06**	0.69± 0.21	0.73±0.12	0.70±0.19	0.60±0.14
0.76±0.16	**0.76±0.10**	0.75± 0.14	0.72±0.11	0.72±0.16	0.62±0.13

better performance than L2S or CV. Dl2S achieves highest improvement in performance of above 65% in one dataset and 42% in an in-vivo dataset. On average, we observe increase in segmentation accuracy by more thab 12% for the all the datasets.

The mean Dice coefficient for each of the dataset is provided in the table. Results obtained using DL2S remain significantly consistent in compariosn to L2S ans Chanvese, for both manual and automatic initialization methods and for all the five different datasets.

A.2 Discussion

We have proposed a novel segmentation method which combines the idea of dictionary learning and region based variational segmentation algorithm in presence of significant clutter and heterogeneous intensity. Furthermore, DL2S outperforms the state of the art in terms of contour initialization and demonstrates accurate segmentation in cluttered images without the use of explicit shape prior. The results presented here show significant improvement in segmentation accuracy using basis functions that are computed from the data in comparison to using a fixed number of basis functions.

Appendix B

Derivation of Tubularity Flow Field equations

We provide the derivation of (6.11) for 2D, ie. $\mathbf{x} = (x, y)^T$. The TuFF vector fields are given by $\mathbf{v}_1 = (v_{11}, v_{12})^T$ and $\mathbf{v}_2 = (v_{21}, v_{22})^T$; the dependency on $\mathbf{x}$ implied. The extension to 3-D is simple and follows from this derivation. We can rewrite $\mathcal{E}_{reg}(\phi) = \int E_1(\phi) d\mathbf{x}$, where $E_1(\phi) = \nu_1 |\nabla\phi(\mathbf{x})| \delta_\epsilon(\phi)$. Then by calculus of variation, the Gateaux variation of $\mathcal{E}_{reg}$ can be obtained as:

$$\frac{\delta\mathcal{E}_{reg}}{\delta\phi} = \frac{\partial E_1}{\partial\phi} - \frac{\partial}{\partial x}\left(\frac{\partial E_1}{\partial\phi_x}\right) - \frac{\partial}{\partial y}\left(\frac{\partial E_1}{\partial\phi_y}\right) \tag{B.1}$$

Since the proof is already shown in [88], we merely state the result as follows:

$$\frac{\delta\mathcal{E}_{reg}}{\delta\phi} = -\nu_1 \mathrm{div}\left(\frac{\nabla\phi}{|\nabla\phi|}\right)\delta_\epsilon(\phi) \tag{B.2}$$

Similarly, we can write the evolution energy as $\mathcal{E}_{evolve}(\phi) = \int E_2(\phi) d\mathbf{x}$. This can be expanded as $E_2(\phi) = A_1(\phi) + A_2(\phi)$, where $A_j(\phi) = \alpha_j \langle \mathbf{v}_j, \frac{\nabla\phi}{|\nabla\phi|} \rangle^2 H_\epsilon(\phi)$. The dependency of α, ϕ and $\mathbf{v}_j$ on $\mathbf{x}$ is implied, and hence not mentioned explicitly.

We can further decompose A_1 as

$$A_1(\phi) = -\alpha_1 \frac{(v_{11}\phi_x + v_{12}\phi_y)^2}{\phi_x^2 + \phi_y^2} H_\epsilon(\phi)$$

Let us denote $\beta_j = \langle \mathbf{v}_j, \mathbf{n} \rangle$, where the unit normal vector $\mathbf{n} = \frac{\nabla\phi}{|\nabla\phi|}$. Therefore, we can write $A_1(\phi) = -\alpha_1 \beta_1^2 H_\epsilon(\phi)$.

As earlier, we compute the Gateaux derivative as follows:

$$\frac{\partial A_1}{\partial \phi} = -\alpha_1 \beta_1^2 \delta_\epsilon(\phi) \tag{B.3}$$

Also, by simple algebraic manipulation, we obtain

$$\frac{\partial A_1}{\partial \phi_x} = -2 \left[\frac{\alpha_1 \beta_1}{|\nabla\phi|} v_{11} - \alpha_1 \left(\frac{\beta_1}{|\nabla\phi|} \right)^2 \phi_x \right] H_\epsilon(\phi)$$

$$\frac{\partial A_1}{\partial \phi_y} = -2 \left[\frac{\alpha_1 \beta_1}{|\nabla\phi|} v_{12} - \alpha_1 \left(\frac{\beta_1}{|\nabla\phi|} \right)^2 \phi_y \right] H_\epsilon(\phi)$$

Therefore, we have

$$\frac{\partial}{\partial x} \left(\frac{\partial A_1}{\partial \phi_x} \right) = -2 \left[\frac{\partial}{\partial x} (\eta_1 v_{11}) - \frac{\partial}{\partial x} \left(\eta_1 \beta_1 \frac{\phi_x}{|\nabla\phi|} \right) \right] \tag{B.4}$$

$$\frac{\partial}{\partial y} \left(\frac{\partial A_1}{\partial \phi_y} \right) = -2 \left[\frac{\partial}{\partial y} (\eta_1 v_{12}) - \frac{\partial}{\partial y} \left(\eta_1 \beta_1 \frac{\phi_y}{|\nabla\phi|} \right) \right] \tag{B.5}$$

Where $\eta_j = \frac{\alpha_j \beta_j}{|\nabla\phi|} H_\epsilon(\phi)$. Therefore, by symmetry we compute

$$\frac{\partial}{\partial x} \left(\frac{\partial A_j}{\partial \phi_x} \right) + \frac{\partial}{\partial y} \left(\frac{\partial A_j}{\partial \phi_y} \right) = -2\mathrm{div} \left[(\eta_j)(\mathbf{v}_j - \beta_j \mathbf{n}) \right] \tag{B.6}$$

The Gateaux variation of $\mathcal{E}_{evolve}$ can be obtained as:

$$\frac{\delta\mathcal{E}_{evolve}}{\delta\phi} = \frac{\partial E_2}{\partial\phi} - \frac{\partial}{\partial x}\left(\frac{\partial E_2}{\partial\phi_x}\right) - \frac{\partial}{\partial y}\left(\frac{\partial E_2}{\partial\phi_y}\right) \tag{B.7}$$

We now use gradient descent to find the local minima of the functionals. The regularizer force and evolution forces are given by $\mathcal{F}_{reg} = -\frac{\delta\mathcal{E}_{reg}}{\delta\phi}$ and $\mathcal{F}_{evolve} = -\frac{\delta\mathcal{E}_{evolve}}{\delta\phi}$ which leads to the following equations:

$$\mathcal{F}_{reg} = \nu_1\text{div}\left(\frac{\nabla\phi}{|\nabla\phi|}\right) \tag{B.8}$$

and

$$\mathcal{F}_{evolve} = \sum_{j=1}^{d}\left(\alpha_j\beta_j^2\delta_\epsilon\left(\phi\right) - 2\text{div}\left[\eta_j\left(\mathbf{v}_j - \beta_j\mathbf{n}\right)\right]\right) \tag{B.9}$$

Bibliography

[1] H. Peng, Z. Ruan, D. Atasoy, and S. Sternson, "Automatic reconstruction of 3d neuron structures using a graph-augmented deformable model," *Bioinformatics*, vol. 26, no. 12, pp. i38–i46, 2010.

[2] A. Rodriguez, D. B. Ehlenberger, P. R. Hof, and S. L. Wearne, "Three-dimensional neuron tracing by voxel scooping," *Journal of Neuroscience Methods*, vol. 184, no. 1, pp. 169–175, 2009.

[3] S. Basu, B. Condron, A. Aksel, and S. T. Acton, "Segmentation and tracing of single neurons from 3d confocal microscope images," *IEEE J. Biomedical and Health Informatics*, vol. 17, no. 2, pp. 319–335, 2013.

[4] H. Peng, "Bioimage informatics: a new area of engineering biology," *Bioinformatics*, vol. 24, no. 17, pp. 1827–1836, 2008.

[5] F. De Chaumont, S. Dallongeville, N. Chenouard, N. Hervé, S. Pop, T. Provoost, V. Meas-Yedid, P. Pankajakshan, T. Lecomte, Y. Le Montagner *et al.*, "Icy: an open bioimage informatics platform for extended reproducible research," *Nature Methods*, vol. 9, no. 7, pp. 690–696, 2012.

[6] J. Schindelin, I. Arganda-Carreras, E. Frise, V. Kaynig, M. Longair, T. Pietzsch, S. Preibisch, C. Rueden, S. Saalfeld, B. Schmid *et al.*, "Fiji: an open-source platform for biological-image analysis," *Nature Methods*, vol. 9, no. 7, pp. 676–682, 2012.

[7] C. A. Schneider, W. S. Rasband, and K. W. Eliceiri, "Nih image to imagej: 25 years of image analysis," *Nature Methods*, vol. 9, no. 7, pp. 671–675, 2012.

[8] J. G. White, E. Southgate, J. N. Thomson, and S. Brenner, "The structure of the nervous system of the nematode caenorhabditis elegans," *Philosophical Transactions of the Royal Society of London. B, Biological Sciences*, vol. 314, no. 1165, pp. 1–340, 1986.

[9] P. V. Belichenko, A. Oldfors, B. Hagberg, and A. Dahlström, "Rett syndrome: 3-d confocal microscopy of cortical pyramidal dendrites and afferents," *Neuroreport*, vol. 5, no. 12, pp. 1509–1513, 1994.

[10] C. Koch and I. Segev, "The role of single neurons in information processing," *Nature Neuroscience*, vol. 3, pp. 1171–1177, 2000.

[11] E. A. Daubert, D. S. Heffron, J. W. Mandell, and B. G. Condron, "Serotonergic dystrophy induced by excess serotonin," *Molecular and Cellular Neuroscience*, vol. 44, no. 3, pp. 297–306, 2010.

[12] J. Chen and B. G. Condron, "Branch architecture of the fly larval abdominal serotonergic neurons," *Developmental biology*, vol. 320, no. 1, pp. 30–38, 2008.

[13] H. Cuntz, F. Forstner, J. Haag, and A. Borst, "The morphological identity of insect dendrites," *PLoS Computational Biology*, vol. 4, no. 12, p. e1000251, 2008.

[14] G. A. Ascoli, D. E. Donohue, and M. Halavi, "Neuromorpho. org: a central resource for neuronal morphologies," *The Journal of Neuroscience*, vol. 27, no. 35, pp. 9247–9251, 2007.

[15] E. Meijering, "Neuron tracing in perspective," *Cytometry Part A*, vol. 77, no. 7, pp. 693–704, 2010.

[16] M. Oberlaender, R. M. Bruno, B. Sakmann, and P. J. Broser, "Transmitted light brightfield mosaic microscopy for three-dimensional tracing of single neuron morphology," *Journal of biomedical optics*, vol. 12, no. 6, pp. 064 029–064 029, 2007.

[17] A. Santamaría-Pang, C. Colbert, P. Saggau, and I. A. Kakadiaris, "Automatic centerline extraction of irregular tubular structures using probability volumes from multiphoton imaging," in *Medical Image Computing and Computer-Assisted Intervention–MICCAI 2007*. Springer, 2007, pp. 486–494.

[18] A. Kreshuk, C. N. Straehle, C. Sommer, U. Koethe, M. Cantoni, G. Knott, and F. A. Hamprecht, "Automated detection and segmentation of synaptic contacts in nearly isotropic serial electron microscopy images," *PloS one*, vol. 6, no. 10, p. e24899, 2011.

[19] A. Dima, M. Scholz, and K. Obermayer, "Automatic segmentation and skeletonization of neurons from confocal microscopy images based on the 3-d wavelet transform," *IEEE Trans. Image Process.*, vol. 11, no. 7, pp. 790–801, 2002.

[20] S. Mukherjee, S. Basu, B. Condron, and S. T. Acton, "Tree2tree2: Neuron tracing in 3d," in *IEEE Intl. Symp. on Biomedical Imaging (ISBI)*, 2012, pp. 448–451.

[21] S. Mukherjee, B. Condron, and S. T. Acton, "Tubularity flow field: A technique for automatic neuron segmentation," *IEEE Trans. Image Process.*, vol. 24, no. 1, pp. 374–389, 2015.

[22] Q. Li, Z. Deng, Y. Zhang, X. Zhou, U. Nagerl, and S. Wong, "A global spatial similarity optimization scheme to track large numbers of dendritic spines in time-lapse confocal microscopy," *IEEE Trans. Med. Imag.*, vol. 30, no. 3, pp. 632–641, March 2011.

[23] Q. Li and Z. Deng, "A surface-based 3-d dendritic spine detection approach from confocal microscopy images," *IEEE Trans. Image Process.*, vol. 21, no. 3, pp. 1223–1230, March 2012.

[24] C. Becker, C. Christoudias, and P. Fua, "Domain adaptation for microscopy imaging," *IEEE Trans. Med. Imag.*, vol. PP, no. 99, pp. 1–1, 2014.

[25] H. Nguyen and Q. Ji, "Shape-driven three-dimensional watersnake segmentation of biological membranes in electron tomography," *IEEE Trans. Med. Imag.*, vol. 27, no. 5, pp. 616–628, 2008.

[26] A. Vaccari, K. Gamage, S. Nachum, B. Condron, C. Deppmann, and S. T. Acton, "Assessment of wallerian degeneration by automated image analysis," in *Asilomar Conf. on Signals, Systems and Computers (ASILOMAR)*. IEEE, 2012, pp. 1583–1587.

[27] S. Mukherjee and S. T. Acton, "Vector field convolution medialness applied to neuron tracing," in *IEEE Intl. Conf. on Image Processing (ICIP)*, 2013, pp. 665–669.

[28] S. Mukherjee and S. Acton, "Region based segmentation in presence of intensity inhomogeneity using legendre polynomials," *IEEE Signal Processing Letters*, vol. 22, no. 3, pp. 298–302, March 2015.

[29] A. F. Frangi, W. J. Niessen, K. L. Vincken, and M. A. Viergever, "Multiscale vessel enhancement filtering," in *Intl. Conf. Medical Image Computing and Computer Assisted Intervention (MICCAI)*. Springer, 1998, pp. 130–137.

[30] Y. S. *et al.*, "Three-dimensional multi-scale line filter for segmentation and visualization of curvilinear structures in medical images," *Medical Image Analysis*, vol. 2, no. 2, pp. 143–168, 1998.

[31] R. M. *et al.*, "Vessel enhancing diffusion: A scale space representation of vessel structures," *Medical Image Analysis*, vol. 10, no. 6, pp. 815–825, 2006.

[32] M. Jacob and M. Unser, "Design of steerable filters for feature detection using canny-like criteria," *IEEE Trans. Pattern Anal. Machine Intell.*, vol. 26, no. 8, pp. 1007–1019, 2004.

[33] A. C. Bovik, *Handbook of Image and Video processing.* Academic press, 2010.

[34] E. Meijering, M. Jacob, J.-C. Sarria, P. Steiner, H. Hirling, and M. Unser, "Design and validation of a tool for neurite tracing and analysis in fluorescence microscopy images," *Cytometry Part A*, vol. 58, no. 2, pp. 167–176, 2004.

[35] A. X. Falcão, J. K. Udupa, S. Samarasekera, S. Sharma, B. E. Hirsch, and R. d. A. Lotufo, "User-steered image segmentation paradigms: Live wire and live lane," *Graphical Models and Image Processing*, vol. 60, no. 4, pp. 233–260, 1998.

[36] M. D. Abràmoff, P. J. Magalhães, and S. J. Ram, "Image processing with imagej," *Biophotonics International*, vol. 11, no. 7, pp. 36–42, 2004.

[37] M. H. Longair, D. A. Baker, and J. D. Armstrong, "Simple neurite tracer: open source software for reconstruction, visualization and analysis of neuronal processes," *Bioinformatics*, vol. 27, no. 17, pp. 2453–2454, 2011.

[38] E. W. Dijkstra, "A note on two problems in connexion with graphs," *Numerische Mathematik*, vol. 1, no. 1, pp. 269–271, 1959.

[39] H. Peng, Z. Ruan, F. Long, J. H. Simpson, and E. W. Myers, "V3d enables real-time 3d visualization and quantitative analysis of large-scale biological image data sets," *Nature Biotechnology*, vol. 28, no. 4, pp. 348–353, 2010.

[40] J. Xie, T. Zhao, T. Lee, E. W. Myers, and H. Peng, "Anisotropic path searching for automatic neuron reconstruction," *Medical Image Analysis*, vol. 15, no. 5, pp. 680–689, 2011.

[41] H. Peng, F. Long, and G. Myers, "Automatic 3d neuron tracing using all-path pruning," *Bioinformatics*, vol. 27, no. 13, pp. i239–i247, 2011.

[42] E. Türetken, G. González, C. Blum, and P. Fua, "Automated reconstruction of dendritic and axonal trees by global optimization with geometric priors," *Neuroinformatics*, vol. 9, no. 2-3, pp. 279–302, 2011.

[43] E. Türetken, F. Benmansour, and P. Fua, "Automated reconstruction of tree structures using path classifiers and mixed integer programming," in *IEEE Conf. on Computer Vision and Pattern Recognition (CVPR)*, 2012, pp. 566–573.

[44] S. Wearne, A. Rodriguez, D. Ehlenberger, A. Rocher, S. Henderson, and P. Hof, "New techniques for imaging, digitization and analysis of three-dimensional neural morphology on multiple scales," *Neuroscience*, vol. 136, no. 3, pp. 661–680, 2005.

[45] Y. Wang, A. Narayanaswamy, C.-L. Tsai, and B. Roysam, "A broadly applicable 3-d neuron tracing method based on open-curve snake," *Neuroinformatics*, vol. 9, no. 2-3, pp. 193–217, 2011.

[46] H. Cai, X. Xu, J. Lu, J. Lichtman, S. Yung, and S. T. Wong, "Shape-constrained repulsive snake method to segment and track neurons in 3d microscopy images," in *IEEE Intl. Symp. on Biomedical Imaging (ISBI)*, 2006, pp. 538–541.

[47] A. Narayanaswamy, Y. Wang, and B. Roysam, "3-d image pre-processing algorithms for improved automated tracing of neuronal arbors," *Neuroinformatics*, vol. 9, no. 2-3, pp. 219–231, 2011.

[48] Y. Y. Boykov and M.-P. Jolly, "Interactive graph cuts for optimal boundary & region segmentation of objects in nd images," in *IEEE Intl. Conf. on Computer Vision (ICCV)*, vol. 1. IEEE, 2001, pp. 105–112.

[49] K. A. Al-Kofahi, A. Can, S. Lasek, D. H. Szarowski, N. Dowell-Mesfin, W. Shain, J. N. Turner, and B. Roysam, "Median-based robust algorithms for tracing neurons from noisy confocal microscope images," *IEEE Trans. Info. Tech. in Biomed.*, vol. 7, no. 4, pp. 302–317, 2003.

[50] R. Srinivasan, X. Zhou, E. Miller, J. Lu, J. Litchman, and S. T. Wong, "Automated axon tracking of 3d confocal laser scanning microscopy images using guided probabilistic region merging," *Neuroinformatics*, vol. 5, no. 3, pp. 189–203, 2007.

[51] J. Wang, X. Zhou, J. Lu, J. Lichtman, S.-F. Chang, and S. T. Wong, "Dynamic local tracing for 3d axon curvilinear structure detection from microscopic image stack," in *IEEE Intl. Symp. on Biomedical Imaging (ISBI)*. IEEE, 2007, pp. 81–84.

[52] A. Choromanska, S.-F. Chang, and R. Yuste, "Automatic reconstruction of neural morphologies with multi-scale tracking," *Frontiers in Neural Circuits*, vol. 6, 2012.

[53] Y. Wang, A. Narayanaswamy, and B. Roysam, "Novel 4-d open-curve active contour and curve completion approach for automated tree structure extraction," in *IEEE Conf. on Computer Vision and Pattern Recognition (CVPR)*. IEEE, 2011, pp. 1105–1112.

[54] D. Lesage, E. D. Angelini, I. Bloch, and G. Funka-Lea, "A review of 3d vessel lumen segmentation techniques: Models, features and extraction schemes," *Medical Image Analysis*, vol. 13, no. 6, pp. 819–845, 2009.

[55] L. M. Lorigo, O. D. Faugeras, W. E. L. Grimson, R. Keriven, R. Kikinis, A. Nabavi, and C.-F. Westin, "Curves: Curve evolution for vessel segmentation," *Medical Image Analysis*, vol. 5, no. 3, pp. 195–206, 2001.

[56] A. Gooya, H. Liao, K. Matsumiya, K. Masamune, Y. Masutani, and T. Dohi, "A variational method for geometric regularization of vascular segmentation in medical images," *IEEE Trans. Image Process.*, vol. 17, no. 8, pp. 1295–1312, 2008.

[57] A. Gooya, H. Liao, and I. Sakuma, "Generalization of geometrical flux maximizing flow on riemannian manifolds for improved volumetric blood vessel segmentation," *Computerized Medical Imaging and Graphics*, vol. 36, no. 6, pp. 474–483, 2012.

[58] A. Vasilevskiy and K. Siddiqi, "Flux maximizing geometric flows," *IEEE Trans. Pattern Anal. Machine Intell.*, vol. 24, no. 12, pp. 1565–1578, 2002.

[59] Y. Shang, R. Deklerck, E. Nyssen, A. Markova, J. de Mey, X. Yang, and K. Sun, "Vascular active contour for vessel tree segmentation," *IEEE Transactions on Biomedical Engineering*, vol. 58, no. 4, pp. 1023–1032, 2011.

[60] B. N. Saha and N. Ray, "Image thresholding by variational minimax optimization," *Pattern Recognition*, vol. 42, no. 5, pp. 843–856, 2009.

[61] S. Osher and J. A. Sethian, "Fronts propagating with curvature-dependent speed: algorithms based on hamilton-jacobi formulations," *Journal of Computational Physics*, vol. 79, no. 1, pp. 12–49, 1988.

[62] V. Caselles, R. Kimmel, and G. Sapiro, "Geodesic active contours," *International Journal of Computer Vision*, vol. 22, no. 1, pp. 61–79, 1997.

[63] M. A. Grayson, "The heat equation shrinks embedded plane curves to round points," *Journal of Differential Geometry*, vol. 26, no. 2, pp. 285–314, 1987.

[64] V. Caselles, R. Kimmel, G. Sapiro, and C. Sbert, "Minimal surfaces based object segmentation," *IEEE Trans. Pattern Anal. Machine Intell.*, vol. 19, no. 4, pp. 394–398, 1997.

[65] A. Tannenbaum, G. Sapiro, and P. J. Olver, "Invariant geometric evolutions of surfaces and volumetric smoothing," *SIAM Journal on Applied Mathematics*, vol. 57, no. 1, pp. 176–194, 1997.

[66] R. Malladi, J. A. Sethian, and B. C. Vemuri, "Shape modeling with front propagation: A level set approach," *IEEE Trans. Pattern Anal. Machine Intell.*, vol. 17, no. 2, pp. 158–175, 1995.

[67] V. Caselles, R. Kimmel, and G. Sapiro, "Geodesic active contours," *International Journal of Computer Vision*, vol. 22, no. 1, pp. 61–79, 1997.

[68] M. Kass, A. Witkin, and D. Terzopoulos, "Snakes: Active contour models," *International Journal of Computer Vision*, vol. 1, no. 4, pp. 321–331, 1988.

[69] B. Li and S. T. Acton, "Active contour external force using vector field convolution for image segmentation," *IEEE Trans. Image Process.*, vol. 16, no. 8, pp. 2096–2106, 2007.

[70] C. Xu and J. L. Prince, "Snakes, shapes, and gradient vector flow," *IEEE Trans. Image Process.*, vol. 7, no. 3, pp. 359–369, 1998.

[71] B. Li and S. T. Acton, "Automatic active model initialization via poisson inverse gradient," *IEEE Trans. Image Process.*, vol. 17, no. 8, pp. 1406–1420, 2008.

[72] M. Jacob, T. Blu, and M. Unser, "Efficient energies and algorithms for parametric snakes," *IEEE Trans. Image Process.*, vol. 13, no. 9, pp. 1231–1244, 2004.

[73] P. Brigger, J. Hoeg, and M. Unser, "B-spline snakes: a flexible tool for parametric contour detection," *IEEE Trans. Image Process.*, vol. 9, no. 9, pp. 1484–1496, 2000.

[74] A. K. Mishra, P. W. Fieguth, and D. A. Clausi, "Decoupled active contour (dac) for boundary detection," *IEEE Trans. Pattern Anal. Machine Intell.*, vol. 33, no. 2, pp. 310–324, 2011.

[75] D. P. Mukherjee, N. Ray, and S. T. Acton, "Level set analysis for leukocyte detection and tracking," *IEEE Trans. Image Process.*, vol. 13, no. 4, pp. 562–572, 2004.

[76] N. Ray, S. T. Acton, T. Altes, E. E. De Lange, and J. R. Brookeman, "Merging parametric active contours within homogeneous image regions for mri-based lung segmentation," *IEEE Trans. Med. Imag.*, vol. 22, no. 2, pp. 189–199, 2003.

[77] N. Ray, S. T. Acton, and K. Ley, "Tracking leukocytes in vivo with shape and size constrained active contours," *IEEE Trans. Med. Imag.*, vol. 21, no. 10, pp. 1222–1235, 2002.

[78] L. Zhu, Y. Gao, V. Appia, A. Yezzi, C. Arepalli, T. Faber, A. Stillman, and A. Tannenbaum, "A complete system for automatic extraction of left ventricular myocardium from ct images using shape segmentation and contour evolution," *IEEE Trans. Image Process.*, vol. 23, no. 3, pp. 1340–1351, 2014.

[79] C. Li, C. Xu, C. Gui, and M. D. Fox, "Level set evolution without re-initialization: a new variational formulation," in *IEEE Conf. on Computer Vision and Pattern Recognition (CVPR)*, vol. 1. IEEE, 2005, pp. 430–436.

[80] ——, "Distance regularized level set evolution and its application to image segmentation," *IEEE Trans. Image Process.*, vol. 19, no. 12, pp. 3243–3254, 2010.

[81] G. Papandreou and P. Maragos, "Multigrid geometric active contour models," *IEEE Trans. Image Process.*, vol. 16, no. 1, pp. 229–240, 2007.

[82] R. Goldenberg, R. Kimmel, E. Rivlin, and M. Rudzsky, "Fast geodesic active contours," *IEEE Trans. Image Process.*, vol. 10, no. 10, pp. 1467–1475, 2001.

[83] J. A. Sethian, "Fast marching methods," *SIAM review*, vol. 41, no. 2, pp. 199–235, 1999.

[84] Y. Shi and W. C. Karl, "A real-time algorithm for the approximation of level-set-based curve evolution," *IEEE Trans. Image Process.*, vol. 17, no. 5, pp. 645–656, 2008.

[85] D. Mumford and J. Shah, "Optimal approximations by piecewise smooth functions and associated variational problems," *Communications on Pure and Applied Mathematics*, vol. 42, no. 5, pp. 577–685, 1989.

[86] J. L. Troutman, *Variational calculus and optimal control: optimization with elementary convexity.* Springer-Verlag New York, Inc., 1995.

[87] H.-K. Zhao, T. Chan, B. Merriman, and S. Osher, "A variational level set approach to multiphase motion," *Journal of Computational Physics*, vol. 127, no. 1, pp. 179–195, 1996.

[88] T. F. Chan and L. A. Vese, "Active contours without edges," *IEEE Trans. Image Process.*, vol. 10, no. 2, pp. 266–277, 2001.

[89] O. Bernard, D. Friboulet, P. Thévenaz, and M. Unser, "Variational b-spline level-set: a linear filtering approach for fast deformable model evolution," *IEEE Trans. Image Process.*, vol. 18, no. 6, pp. 1179–1191, 2009.

[90] S. Lankton and A. Tannenbaum, "Localizing region-based active contours," *IEEE Trans. Image Process.*, vol. 17, no. 11, pp. 2029–2039, 2008.

[91] T. Chan and W. Zhu, "Level set based shape prior segmentation," in *IEEE Conf. on Computer Vision and Pattern Recognition (CVPR)*, vol. 2, 2005, pp. 1164–1170.

[92] D. Cremers, M. Rousson, and R. Deriche, "A review of statistical approaches to level set segmentation: integrating color, texture, motion and shape," *International Journal of Computer Vision*, vol. 72, no. 2, pp. 195–215, 2007.

[93] A. Foulonneau, P. Charbonnier, and F. Heitz, "Affine-invariant geometric shape priors for region-based active contours," *IEEE Trans. Pattern Anal. Machine Intell.*, vol. 28, no. 8, pp. 1352–1357, 2006.

[94] D. Nain, A. Yezzi, and G. Turk, "Vessel segmentation using a shape driven flow," in *Medical Image Computing and Computer-Assisted Intervention–MICCAI 2004*. Springer, 2004, pp. 51–59.

[95] L. A. Vese and T. F. Chan, "A multiphase level set framework for image segmentation using the mumford and shah model," *International Journal of Computer Vision*, vol. 50, no. 3, pp. 271–293, 2002.

[96] S. Basu, A. Aksel, B. Condron, and S. T. Acton, "Tree2tree: Neuron segmentation for generation of neuronal morphology," in *IEEE Intl. Symp. on Biomedical Imaging (ISBI)*, 2010, pp. 548–551.

[97] C. Li, C.-Y. Kao, J. C. Gore, and Z. Ding, "Minimization of region-scalable fitting energy for image segmentation," *IEEE Trans. Image Process.*, vol. 17, no. 10, pp. 1940–1949, 2008.

[98] J. Kim, J. W. Fisher, A. Yezzi, M. Çetin, and A. S. Willsky, "A nonparametric statistical method for image segmentation using information theory and curve evolution," *IEEE Trans. Image Process.*, vol. 14, no. 10, pp. 1486–1502, 2005.

[99] H. Feng, D. A. Castanon, and W. C. Karl, "Tomographic reconstruction using curve evolution," in *IEEE Conf. on Computer Vision and Pattern Recognition (CVPR)*, vol. 1, 2000, pp. 361–366.

[100] X. Du and T. D. Bui, "A new model for image segmentation," *IEEE Signal Processing Letters*, vol. 15, pp. 182–185, 2008.

[101] K. D. Fritscher, A. Grünerbl, and R. Schubert, "3d image segmentation using combined shape-intensity prior models," *International Journal of Computer Assisted Radiology and Surgery*, vol. 1, no. 6, pp. 341–350, 2007.

[102] X. Huang and D. N. Metaxas, "Metamorphs: deformable shape and appearance models," *IEEE Trans. Pattern Anal. Machine Intell.*, vol. 30, no. 8, pp. 1444–1459, 2008.

[103] N. Barth, "The gramian and k-volume in n-space: some classical results in linear algebra," *J Young Investig*, vol. 2, 1999.

[104] T. Dietenbeck, M. Alessandrini, D. Friboulet, and O. Bernard, "Creaseg: a free software for the evaluation of image segmentation algorithms based on level-set," in *IEEE Intl. Conf. on Image Processing (ICIP)*, 2010, pp. 665–668.

[105] D. Martin, C. Fowlkes, D. Tal, and J. Malik, "A database of human segmented natural images and its application to evaluating segmentation algorithms and measuring ecological statistics," in *IEEE Intl. Conf. on Computer Vision (ICCV)*, vol. 2, July 2001, pp. 416–423.

[106] A. Achuthan, M. Rajeswari, D. Ramachandram, M. E. Aziz, and I. L. Shuaib, "Wavelet energy-guided level set-based active contour: A segmentation method to segment highly similar regions," *Computers in biology and medicine*, vol. 40, no. 7, pp. 608–620, 2010.

[107] R. Sarkar, S. Mukherjee, and S. Acton, "Dictionary learning level sets (*accepted*)," *IEEE Signal Processing Letters*, 2015.

[108] M. Aharon, M. Elad, and A. Bruckstein, "-svd: An algorithm for designing overcomplete dictionaries for sparse representation," *IEEE Trans. Signal Process.*, vol. 54, no. 11, pp. 4311–4322, 2006.

[109] N. Otsu, "A threshold selection method from gray-level histograms," *Automatica*, vol. 11, no. 285-296, pp. 23–27, 1975.

[110] R. L. Graham and F. Frances Yao, "Finding the convex hull of a simple polygon," *Journal of Algorithms*, vol. 4, no. 4, pp. 324–331, 1983.

[111] S. T. Acton, "Fast algorithms for area morphology," *Digital Signal Processing*, vol. 11, no. 3, pp. 187–203, 2001.

[112] K. M. Brown, G. Barrionuevo, A. J. Canty, V. De Paola, J. A. Hirsch, G. S. Jefferis, J. Lu, M. Snippe, I. Sugihara, and G. A. Ascoli, "The diadem data sets: representative light microscopy images of neuronal morphology to advance automation of digital reconstructions," *Neuroinformatics*, vol. 9, no. 2-3, pp. 143–157, 2011.

[113] J. Wright, A. Y. Yang, A. Ganesh, S. S. Sastry, and Y. Ma, "Robust face recognition via sparse representation," *IEEE Trans. Pattern Anal. Machine Intell.*, vol. 31, no. 2, pp. 210–227, 2009.

[114] K. Kreutz-Delgado, J. F. Murray, B. D. Rao, K. Engan, T.-W. Lee, and T. J. Sejnowski, "Dictionary learning algorithms for sparse representation," *Neural Computation*, vol. 15, no. 2, pp. 349–396, 2003.

[115] M. Elad and M. Aharon, "Image denoising via sparse and redundant representations over learned dictionaries," *IEEE Trans. Image Process.*, vol. 15, no. 12, pp. 3736–3745, 2006.

[116] J. Mairal, F. Bach, J. Ponce, G. Sapiro, and A. Zisserman, "Non-local sparse models for image restoration," in *IEEE Conf. on Computer Vision and Pattern Recognition (CVPR)*. IEEE, 2009, pp. 2272–2279.